Environmental Science and Pollution Research (2021) 28:45414–45421
https://doi.org/10.1007/s11356-021-13436-1

RESEARCH ARTICLE

Mechanism insight into the role of clay particles on enhancing phosphate removal by ferrate compared with ferric salt

Wentao Li[1] · Fan Ouyang[1] · Guangyu An[2] · Chenggang Yang[3] · Runsheng Zhong[1] · Feng Xiao[1,4] · Dan Peng[1] · Dongsheng Wang[2]

Received: 28 October 2020 / Accepted: 9 March 2021 / Published online: 17 April 2021
© The Author(s), under exclusive licence to Springer-Verlag GmbH Germany, part of Springer Nature 2021

Abstract

The application of ferrate (Fe(VI)) and ferric chloride as coagulants for treating phosphate wastewater in the presence of kaolin clay particles was comparatively studied. The phosphate removal processes by ferrate and ferric chloride assisted with kaolin clay particles were investigated under different Fe/P molar ratios. At neutral pH, complete removal of phosphates by ferrate and ferric chloride was observed at 2:1 and 6:1 of Fe/P molar ratio, respectively. The effect of kaolin clay particles on the phosphate removal process was discussed by zeta potential, size particle distribution, FTIR and XPS. We showed that with the increase of Fe/P molar ratio, the interaction intensity of kaolin clay particles with Fe flocs was decreased by ferric chloride coagulation while firstly increased and then decreased by ferrate. This depends on the Fe species with positive charge from ferric chloride hydrolysis and ferrate decomposition. Phosphate can inhibit the formation of $FeOH^{2+}$ and $Fe(OH)_2^+$ in the ferric chloride hydrolysis but promote the formation of FeOOH and $Fe(OH)_2^+$ in the ferrate decomposition. Kaolin clay particles can more remarkably promote phosphate removal by ferrate than by ferric chloride.

Keywords Fe(VI) · Ferric chloride · Coagulation mechanism · Kaolin particles · Particle size · Fe species · Phosphate removal process

Introduction

Phosphorus is an essential nutrient for all living forms, naturally found in freshwater or waste water. However, high phosphate concentration can stimulate the growth of organisms, leading to the formation of algal bloom that may pose a risk to human health (Nakarmi et al. 2020; Yu et al. 2020). Anthropogenic behaviours are main sources, including agricultural runoff and industrial discharge (Ahmad et al. 2020; Vikrant et al. 2018). Phosphates are firstly transferred into sedimentation and then released into water bodies (Lin and Chen 2021; Zhao et al. 2020). The natural recovery rate of phosphate is extremely slow. Therefore, it is important to control the phosphate concentration in the waters.

The current chemical methods for phosphate removal in freshwater are mainly divided into two categories, as following: sorption and chemical precipitation (Hu et al. 2020; Yang et al. 2018; Wu et al. 2019). Many materials, used as adsorbents to remove the phosphate by metal–phosphate complex (i.e. $\equiv FePO_4^{2-}$), have been reported in previous literatures (Zhang et al. 2016; Wang et al. 2019; Zhang et al. 2020a, b; Xu et al. 2020; Yasipourtehrani et al. 2019), including nano-La(III) oxides, aluminium hydroxide, iron-based materials and blast furnace slag. These adsorbents are costly or had undesirable adsorption capabilities, such as 100:1 to10:1 of sorbent to phosphate mass ratios (Wilfert et al. 2015; Li et al. 2013). Large volumes of sludge and wastewater after phosphate desorption are produced, leading to high cost of treatment. More importantly, additional factors (i.e. bicarbonates, silicate and NOM) can decrease the phosphate adsorption efficiency by sorbents (Deng et al. 2019; Lin et al. 2017; Cho

Responsible Editor: Philipp Gariguess

✉ Runsheng Zhong
runsoon@qq.com

[1] Shenzhen Institute of Information Technology, Shenzhen 518172, China

[2] Research Center for Eco-Environmental Sciences, Chinese Academy of Sciences, Beijing 100085, China

[3] Nuclear and Radiation Safety Centre MEE, Beijing 102400, China

[4] School of Renewable Energy, North China Electric Power University, Beijing 102206, China

et al. 2019). With regard to chemical precipitation, phosphate can be removed using aluminium or iron-based coagulants (Chu et al. 2019; Inan and Alaydin 2014). The performance of hydrolyzing aluminium or iron coagulants is affected by complexed anions, such as phosphate or silicate (Lartiges et al. 2019).

Ferrate often has been used as a high-effective and green chemical agent for removing various inorganic contaminants (Dong et al. 2019; Kralchevska et al. 2016). The advantage of ferrate arises from oxidation and subsequent coagulation by γ-Fe_2O_3 (Prucek et al. 2015). There are a handful of studies reported in the literatures on the effective coagulation of toxic organic compounds and phosphate by ferrate (Yang et al. 2020; Wang et al. 2020; Kralchevska et al. 2016). Phosphates were completely removed by ferrate from water at 5 Fe/P mass ratio (Kralchevska et al. 2016). Compared with phosphate removal by ferric chloride with 7 Fe/P ratio, it is significantly improved by ferrate. This is related largely with coagulation process. The effect of clay particles on phosphate removal by ferrate and ferric chloride is unknown, especially for the interaction between ferrate and clay particles.

This paper compared the phosphate removal processes by ferrate and ferric chloride at neutral pH and investigated the intricate relationship between simple aggregation descriptors and the nature of coagulant species. From the interfacial characteristics of particulate matter (i.e. zeta potential, size distribution, FTIR and XPS), the impact of kaolin clay particles on phosphate removal by ferrate and ferric chloride coagulation was analysed.

Experiments

Chemicals

Kaolin(1–5 um, negative charge), sodium bicarbonate, sodium phosphate dibasic and ferric chloride hexahydrate were purchased from Sigma-Aldrich or Sinopharm Chemical Reagent Co., Ltd. Potassium (K_2FeO_4, > 90%) was prepared by hypochlorite oxidation of ferric nitrate according to the method of Delaude and Laszlo (Inan and Alaydin 2014).

Synthetic test water was prepared by adding a measured amount of 0.2 mol/L Na_2HPO_4 stock solution into deionized water (0–0.2 mM P). Meanwhile, 1 mM $NaHCO_3$ was added to provide a certain buffer capacity and ionic strength as well as 50 mg/L kaolin. The pH of test water was adjusted by 0.1 mol/L NaOH or 0.1 mol/L HNO_3 solutions.

Jar test

Standard jar tests were conducted on a programme-controlled jar test apparatus (TA-6, Wuhan Hengling Technology Co. Ltd., China) at room temperature. The coagulation process was as follows: (1) a test water of 300 ml was transferred into a 500-ml beaker; (2) 0.2 mmol/L ferrate or ferric chloride was dosed to pretreatment under rapid stirring of 250 rpm for 0.5 min, followed by a rapid mix at 200 rpm for 1 min; (3) after 1.5 min, the stirring speed was changed to 40 rpm with a duration of 10 min; and (4) after 30 min of quiescent settling, the sample was collected from 2 cm below the surface for measurements. The collected sample was filtered through a 0.45-um membrane to measure the P concentration, final pH and turbidity.

Analysis

The morphologies of kaolin and Fe flocs were measured by field emission scanning electron microscope (FESEM, scanning voltages 10 kV) (SU-8020, Hitachi Limited). X-ray photoelectron spectroscopy with Al-K X-ray irradiation (ESCALAB 250Xi, Thermo Fisher Scientific) was used to examine the surface properties of flocs. Infrared spectrums of Fe flocs were recorded with an ATR-FTIR spectrophotometer (Nicolet 8700, Thermo Fisher Scientific). Zeta potential and size distribution of Fe flocs were measured by using Zetasizer NanoZS (Malvern Instrument Ltd., Worcestershire, UK). The total P concentration was determined from the absorbance at the wavelength of 700 nm by an UV-visible spectrophotometer (UV-2990, Shimadzu, Japan). The pH of all solutions was read by a Mettler Toledo pH meter (FE20) with a combined glass electrode (LE438). The turbidity was measured using a 2100N turbidimeter (Hach, USA).

Results and discussion

Phosphate removal by ferrate and ferric chloride

The phosphate (P) removal efficiency, turbidity and Fe residual amount using ferrate and ferric chloride coagulation were comparatively investigated under neutral pH. Figure 1 showed the variation of P removal efficiency, turbidity and Fe residual amount as a function of the molar ratio of phosphate to iron (P/Fe). For P removal by ferrate, when the molar ratio of P to Fe was increased from 0 to 0.5, P removal efficiency and Fe residual amount in solution were 100% and 0, respectively, and turbidity was decreased from 25 to 0 NTU. When the P/Fe molar ratio was increased from 0.5 to 0.83, P removal efficiency was decreased from 100% to around 10%, and turbidity and Fe residual amount were increased from 0 to 70 NTU and from 0 to 13 mg/L, respectively. At more than 0.83 P/Fe molar ratio, P removal efficiency, turbidity and Fe residual amount were almost no changed.

For ferric chloride coagulation, at less than 0.17 P/Fe ratio, the efficiency of P removal was kept at 100%, and both turbidity and Fe residual amount in solution were 0. With the

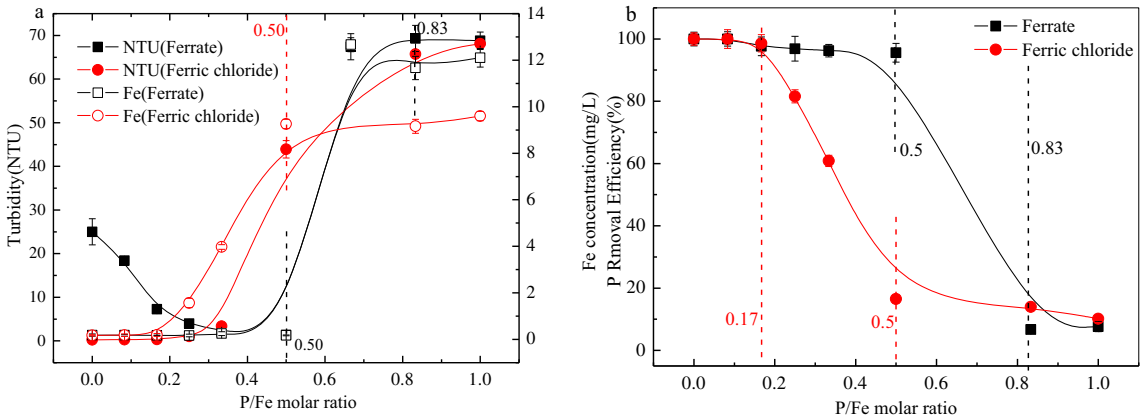

Fig. 1 Phosphate removal by ferrate and ferric chloride under different P/Fe molar ratios: **a** Fe concentration and remaining turbidity; **b** *P* removal efficiency (ferrate or ferric chloride dosage, 0.2 mM; phosphate concentration, 0–0.2 mM; kaolin dosage, 50 mg/L; pH, neutral)

increase of the P/Fe ratio from 0.17 to 0.5, P removal efficiency started down from 100% to 10%, and turbidity and Fe residual amount were increased from 0 to 65 NTU and from 0 to 9mg/L. When the P/Fe molar ratio was higher than 0.83, P removal efficiency, turbidity and Fe residual amount were almost kept stable. By comparison of ferrate and ferric chloride coagulation, we found that (1) P removal efficiency, Fe residual amount and turbidity were around 100%, 0 and decreased from 25 to 0 NTU by ferrate at less than one-half of the P/Fe molar ratio while being 100, 0 and 0 by ferric chloride at less than 1:6 of the P/Fe molar ratio, respectively; (2) the variations of P removal efficiencies, turbidity and Fe residual amount were similar at more than one-half of the P/Fe ratio for ferrate coagulation and at more than one-sixth of the P/Fe ratio for ferric chloride coagulation, respectively. This may result from the different mechanisms of P removal by ferrate or ferric chloride. Compared with previous reports with a 5:1 Fe/P molar ratio for ferrate (Kralchevska et al. 2016) and a 7:1 Fe/P molar ratio for ferric chloride (Lartiges et al. 2019), this result was improved significantly. This should be related with kaolin addition.

Zeta potential and flocs' size analysis

The surface charge of Fe flocs with or without the kaolin clay under different P/Fe molar ratios was investigated using the zeta potential analyser (Fig. 2). Generally, phosphate concentration has a large influence on the surface charge of iron oxides due to the inner Fe–P complex formation (Lartiges et al. 2019), leading to the change of zeta potential from positive to negative with the increase of phosphate concentration. In the process of ferric chloride coagulation, kaolin clay particles quickly reduced the zeta potential of this system. For example, zeta potential was decreased from −6 to −16 mv at 0.1 P/Fe molar ratio after kaolin addition. Interestingly, in the ferrate coagulation system, zeta potentials in the solution at less than 0.1 P/Fe molar ratio were almost the same with or without kaolin particles in the solution. With the increase of P/Fe molar ratio, difference of zeta potential with or without kaolin was larger and larger in the ferrate coagulation, especially with more than 0.6 P/Fe ratio. This indicates that the chemical interaction between Fe flocs and kaolin in the presence of phosphate at low molar ratio of P/Fe is weaker in ferrate coagulation than that in ferric chloride coagulation.

The particle size distribution of Fe flocs with or without kaolin under different P/Fe ratios on ferrate coagulation and ferric chloride coagulation measured using the laser diffraction instrument are shown in Fig. 3. The results indicate that Fe flocs size had a diameter of around 800 um on ferric chloride coagulation without phosphate (Fig. 3a). With the increase of P/Fe molar ratio, flocs' size became gradually smaller, especially at more than 0.5 P/Fe molar ratio (round 30 um of particle size). This suggests that phosphate inhibits the growth of particles. Compared with ferric chloride, the particle

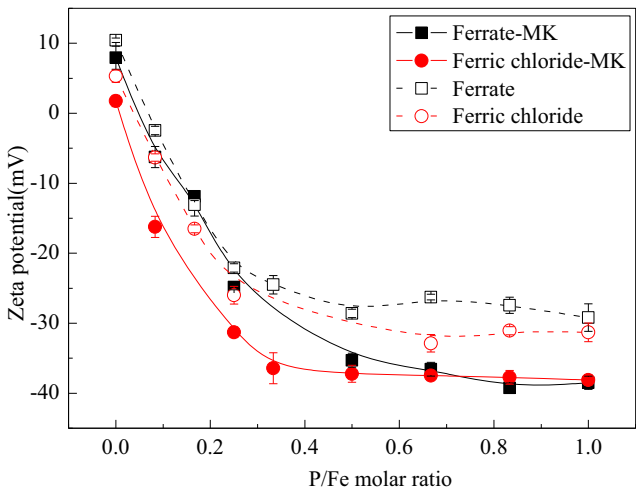

Fig. 2 Zeta potential of Fe flocs after ferric chloride hydrolysis and ferrate decomposition with or without kaolin at neutral pH ([Fe] = 0.2 mM, [kaolin] = 50 mg/L, [P] = 0–0.2 mM)

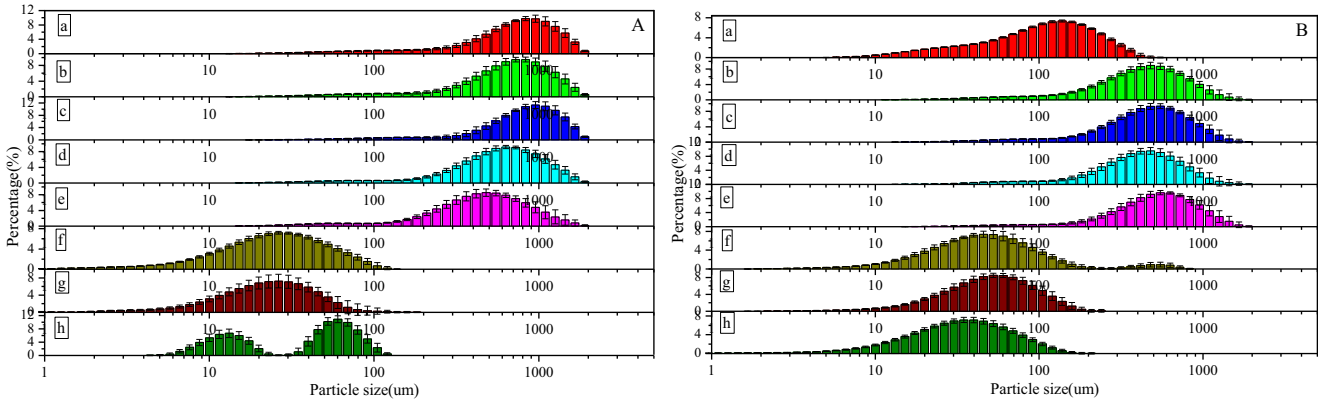

Fig. 3 Particle size distribution after ferric chloride (**a**) and ferrate (**b**) coagulation at neutral pH under different molar ratios of phosphate to Fe ([Fe] = 0.2 mM, [P]/[Fe] = 0 (a), 0.083 (b), 0.17 (c), 0.25 (d), 0.33 (e),0.50 (f),0.67 (g),1 (h))

size of Fe flocs on ferrate coagulation without phosphate had a diameter between 100 and 200 um (Fig. 3b), which was significantly lower than that on ferric chloride coagulation. When P/Fe molar ratio was increased, Fe flocs' size was gradually increased and then decreased. At more than 0.5 P/Fe molar ratio, Fe flocs size was 40–50 um.

Characteristics of flocs particles

FTIR

To investigate the special interaction among phosphate, kaolin and ferrate (or ferric chloride), FTIR spectra of Fe flocs obtained by ferrate and ferric chloride coagulation were measured. FTIR spectrum of kaolin (Fig. S1) showed characteristic bands of kaolinite at 1114, 1025, 996, 934, 909, 789 and 749 cm^{-1}. Bands of 789 and 749cm^{-1} were assigned to the Si–O–Al compounded vibrations (Saikial and Parthasarathy 2010). In the Si–O region, stretching vibrations bands at 1114, 1025, 996 cm^{-1} were noticed (Ilić et al. 2016). In addition, both 934 and 909 cm^{-1} corresponded Al–OH bending vibration (Saikial and Parthasarathy 2010). Fig. 4a exhibited the FTIR spectra of Fe flocs produced by ferrate under different P/Fe molar ratios. In the absence of phosphate, the IR spectra of flocs obtained from ferrate were almost the same with that of kaolin. Bouzek (Bouzek et al. 1999) reported that intermediate products appeared in the transformation of Fe(VI) to $Fe(OH)_3$, such as FeO_4^{4-}/FeO_3^{3-}, which may inhibit the interaction between ferrate and kaolin. With the increase of P/Fe molar ratio, the peak at 996 cm^{-1} obviously shifted towards high wavenumber. For instance, when P/Fe molar ratio was 0.5, it appeared at 1000 cm^{-1}. This results from the formation of Si–O–Fe on the surface of kaolin (Doelsch et al. 2001). Charfi (Charfi et al. 2013) found that phosphate could react with kaolin such as new mineral phase formation. While the P/Fe molar ratio exceeded 0.5, the peak shifted from 1000 to 996 cm^{-1}. Too much phosphate may complex with products from ferrate, limiting the formation of Fe–O–Si. Huang (Huang et al. 2018) reported that phosphate ligand could restrain the Fe(V) complex to associate with target compounds.

In the FTIR spectrum of Fe flocs produced by ferric chloride without phosphate (Fig. 4b), the band of 1000 cm^{-1}, which is attributed to the Si–O–Fe vibration, was readily found, because Fe^{3+} was intensely adsorbed on the surface

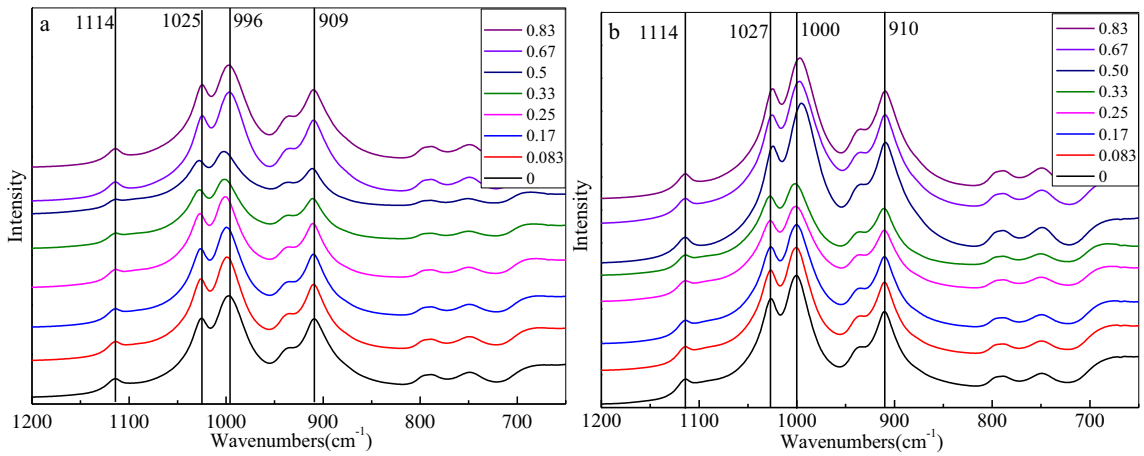

Fig. 4 FTIR spectra of Fe flocs produced from 200 uM ferrate (**a**) and ferric chloride (**b**) with 50 mg/L kaolin under different P/Fe ratio (0–0.83)

of kaolin with negative charge. As the P/Fe molar ratio was raised, the interaction of kaolin and Fe became weaker because of the complexation between Fe and phosphate. When the P/Fe molar ratio increased from 0.33 to 0.5, the peak position changed from 1000 to 996 cm^{-1}, leading that the complex of P–Fe entered into the solution.

XPS

The XPS technique was used to further confirm the surface chemical composition of Fe flocs' particles. The results (Fig. S2) displayed that Fe flocs mainly included the elements of Fe, P, Si, O and Al. The binding energy of Fe 2p3/2 in the Fe flocs produced by ferrate without phosphate was round 710.8 eV, while around 711.5 eV in the Fe flocs was produced by ferrate with phosphate, as shown in Fig. S3. The binding energy of Fe 2p3/2 was 711.5 eV in the Fe flocs obtained from ferric chloride with or without phosphate. The high-resolution XPS spectra of Fe 2p3/2 in Fe flocs (Fig. 5) were fitted into three peaks, namely, 710.9 eV for Fe–O–Fe, 711.9 eV for Fe–O–Si and 713.3 eV for Fe–O–P, listed in Table S1. In the Fe flocs from ferrate, the predominant species in the absence of phosphate was the Fe–O–Fe bond (97.2%, percentage in Fe atom), while 24.0% of Fe–O–Si at 0.33 P/Fe molar ratio appeared on the surface of Fe flocs, demonstrating that phosphate addition can increase the interaction between kaolin and products after ferrate decomposition. For the Fe flocs from ferric chloride, percentages of Fe–O–Si were 45.1 and 36.8% in the absence and presence of phosphate, respectively. In contrast, phosphate addition can decrease the interaction between kaolin and products after ferric chloride hydrolysis.

SEM

The morphology and structure of Fe flocs obtained from ferrate and ferric chloride coagulation were investigated, and the results (Figs. S4 and S5) exhibited that Fe flocs were formed with different P/Fe molar ratios (0–1.0) at neutral pH. It found that more Fe flocs were formed and attached to the surface of kaolin with the increase of the P/Fe molar ratio, but the growth of flocs from ferrate and ferric chloride was inhibited at 1.0 and 0.5 P/Fe molar ratios, respectively. Differently, Fe flocs produced by decomposition of ferrate at 0.33 P/Fe ratio displayed the ultrafine nanosphere-stacking structure, while Fe flocs formed by the hydrolysis of Fe chloride showed the porous and disorder structure (Fig. 6). This indicates that there are some differences for coagulation mechanisms of ferrate and Fe chloride. In the ferric chloride coagulation, the binding of a phosphate ligand terminating the growth of polymeric chains of edge-sharing Fe octahedra and those non-equilibrium nanosized Fe–P coagulant species assembles the silica nanoparticles to form hetero-aggregates (Lartiges et al. 2019), while in the ferrate coagulation, phosphate was removed from water solely by sorption on the

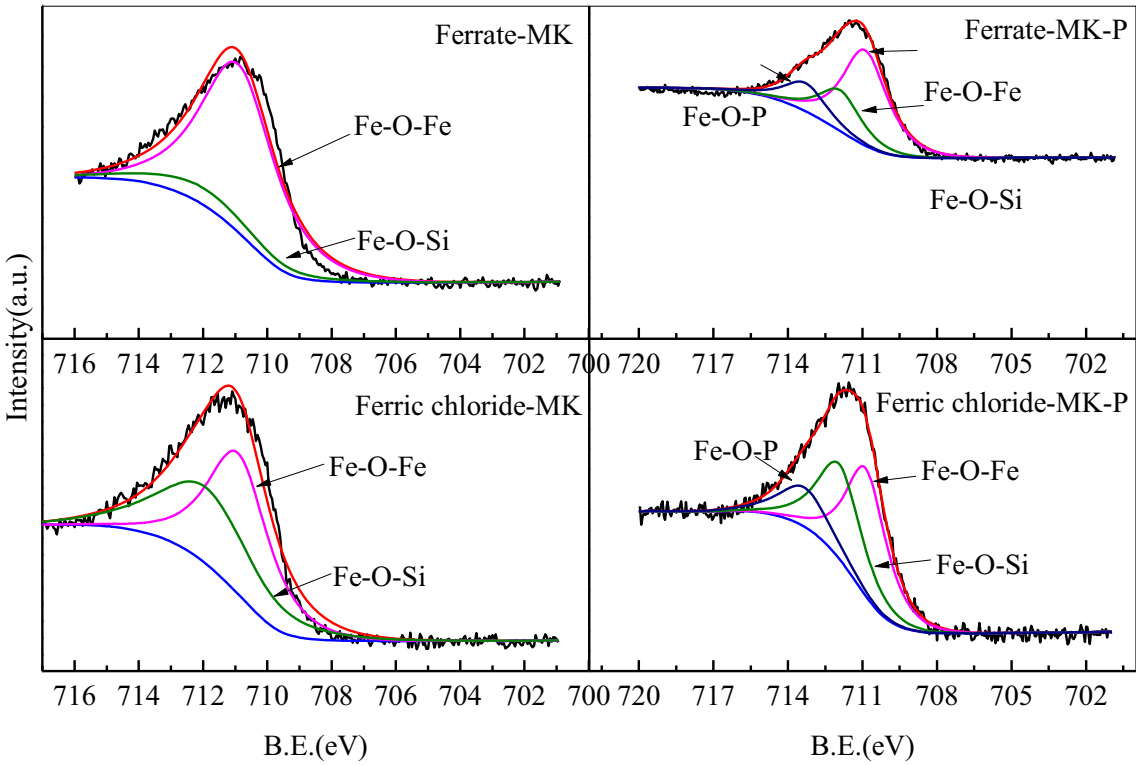

Fig. 5 High-resolution XPS spectra of Fe2p3/2 in Fe flocs obtained using ferrate or Fe chloride with or without phosphate (P/Fe 0.33) in the presence of kaolin

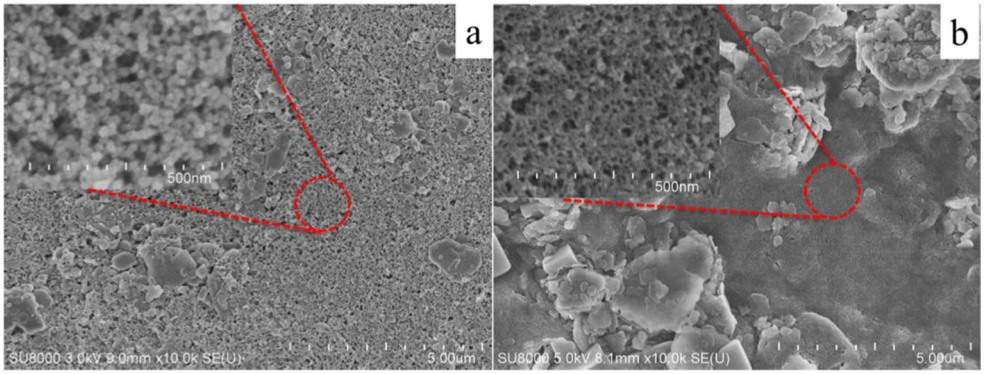

Fig. 6 FESEM images of Fe-phosphate flocs obtained by ferrate (**a**) or Fe chloride (**b**) co-agulation (0.33 P/Fe ratio)

surface from γ-Fe_2O_3/γ-FeOOH nanoparticles (Kralchevska et al. 2016).

Mechanism analysis

Phosphate removal mechanism

The ferrate (FeO_4^{2-}) decomposition mechanism at pH 7–9 is listed in Eqs. (1) to (3) (Chen et al. 2018). The transformation of Fe(VI) to Fe(III) can produce active species of Fe(III), including FeO_2^-, FeO(OH) and $Fe(OH)_2^+$. From charge point, FeO(OH) and $Fe(OH)_2^+$ are the main adsorptive sites for phosphate removal (Antelo et al. 2005; Chitrakar et al. 2006), which derive from the reaction of FeO_2^- with proton (Eqs. (2) and (3)). Phosphates are removed from water by sorption on the surface of FeOOH nanoparticles produced from ferrate (Kralchevska et al. 2016). Phosphate removal by ferric chloride has the relation with hydrolytic pathway of Fe(III). In the hydrolysis process, the reaction of Fe^{3+} with hydroxyl ion can form $Fe(OH)^{2+}$, $Fe(OH)_2^+$ and $Fe(OH)_3$ species in the solution. At neutral condition, $Fe(OH)_2^+$ and $Fe(OH)_3$ are the main active sites for phosphate adsorption. Phosphates are removed by Fe oligomers linked by phosphate tetrahedral (Fe–P complex) on the ferric chloride coagulation (Lartiges et al. 2019).

$$2FeO_4^{2-} + H_2O \rightarrow 2FeO_2^- + \frac{3}{2}O_2 + OH^- \quad (1)$$

$$FeO_2^- + H_2O \rightarrow FeO(OH) + OH^- \quad (2)$$

$$FeO(OH) + H_2O \rightarrow Fe(OH)_2^+ + OH^- \quad (3)$$

$$Fe^{3+} + H_2O \rightarrow Fe(OH)^{2+} + H^+ \quad (4)$$

$$Fe(OH)^{2+} + H_2O \rightarrow Fe(OH)_2^+ + H^+ \quad (5)$$

$$Fe(OH)_2^+ + H_2O \rightarrow Fe(OH)_3 + H^+ \quad (6)$$

According to the phosphate species distribution, $H_2PO_4^-$ and HPO_4^{2-} are the dominative species at pH 7. The dissociation constants of $H_2PO_4^-$ and HPO_4^{2-} are 6.2×10^{-8} and 2.2×10^{-13}(Cameron and Liss 1984), respectively, which are higher than that of H_2O (10^{-14}). Generally, the dissociation constant is greater, and proton is generated more easily. $H_2PO_4^-$ and HPO_4^{2-} can easily form more protons than H_2O molecules. In the chemical equilibrium of Eqs. (1)to (3), phosphate promotes ferrate decomposition and produces much more FeO(OH) and $Fe(OH)_2^+$. In contrast, phosphate inhibits the hydrolysis of ferric chloride (Eqs. (4) to(6)), even terminating the formation of $Fe(OH)_2^+$ and $Fe(OH)_3$.

Effect mechanism of kaolin particles

The relationship of interaction between kaolin clay particles and Fe flocs is expressed by 1/NTU, as shown in Fig. 7. With the increase of Fe/P molar ratio, the interaction of kaolin-Fe flocs from ferric chloride coagulation became

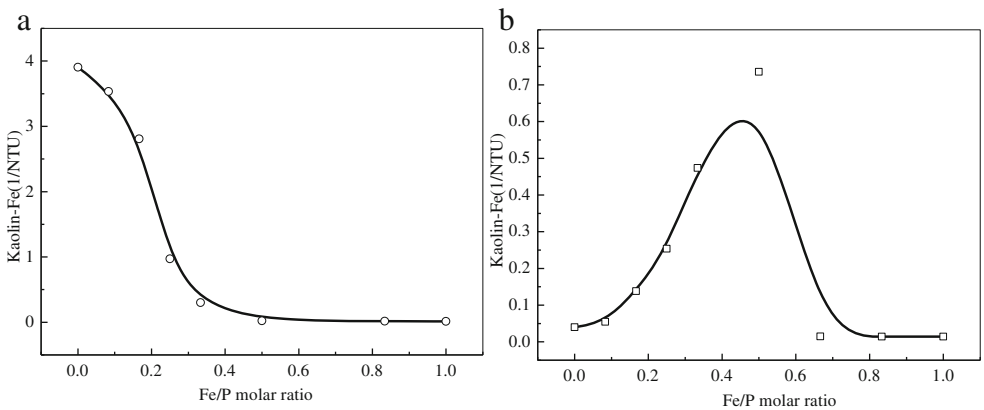

Fig. 7 Relationship between kaolin-Fe and Fe/P molar ratio: **a** ferric chloride and **b** ferrate

weaker, while the interaction from ferrate coagulation became stronger and then weaker. It is suggested that phosphate could promote the aggregate of kaolin and Fe flocs on the ferrate coagulation while decreasing it on the ferric chloride coagulation. This may be attributed that $Fe(OH)_2^+$ can be produced in the presence of phosphate in the ferrate decomposition by Eq. (2), which can strongly adsorb on the surface of kaolin.

In the neutral solution, Fe(VI) is decomposed into many species with negative or neutral charges, such as FeO_4^{2-}, FeO_4^{4-}, FeO_3^{2-}, FeO_2^{2-}, FeO(OH) and $Fe(OH)_3$, which have some rejection with kaolin clay particles. Compared with ferric chloride, when ferric chloride is dissolved into the solution, Fe^{3+}, $Fe(OH)^{2+}$ and $Fe(OH)_2^+$ are produced, which are adsorbed on the surface of kaolin clay because of electrostatic attraction. In kaolin alone, the size of Fe flocs from ferric chloride coagulation is far larger than that from ferrate coagulation (Fig. 3). With the increase of P/Fe molar ratio, the amount of $Fe(OH)_2^+$ on ferrate coagulation is rapidly increased, leading to the increase of electrostatic attraction between kaolin and ferrate decomposition products. Therefore, the size of Fe flocs from ferrate is raised with phosphate addition. In contrast, on ferric chloride coagulation, Fe species binding with kaolin may be reduced due to phosphate competition, decreasing the Fe flocs' size. When the P/Fe molar ratio arrived at certain value (0.67 for ferrate and 0.5 for ferric chloride), Fe flocs' sizes decreased the lowest. Because Fe in the solution almost complexes with phosphate instead of kaolin clay.

Conclusion

The comparison of phosphate removal by ferrate and ferric chloride was studied in the presence of kaolin particles. Phosphate was completely removed at 2:1 (ferrate) and 6:1 (ferric chloride) of the Fe/P molar ratio, which was improved than previous reports with 5:1 of the Fe/P molar ratio for ferrate (Kralchevska et al. 2016) and 7:1 of the Fe/P molar ratio for ferric chloride (Lartiges et al. 2019). The characteristics of aggregates formed were described using a combination of techniques, i.e. zeta potential and particle size distribution, FTIR and XPS. We found that the interaction intensity (i.e. Fe–O–Si) between ferric chloride and kaolin was decreased with the increase of phosphate concentration while firstly increased and then decreased between ferrate and kaolin. This may have a large relation with Fe species produced in the ferric chloride hydrolysis and ferrate decomposition. From charge point, phosphate can inhibit the interaction between kaolin and Fe species from ferric chloride because of Fe–P complexion while increasing the interaction between kaolin and Fe species from ferrate due to electrostatic attraction. Therefore, kaolin particles can significantly promote the phosphate removal by ferrate.

Supplementary Information The online version contains supplementary material available at https://doi.org/10.1007/s11356-021-13436-1.

Acknowledgements Not applicable.

Author contribution WL played a major role in writing the original draft, editing and conceptualization. RZ and FX designed the experiments and writing—review and editing. FO and GA performed the experiments. CY, DP and DW analysed and interpreted the data regarding the interaction between phosphate and Fe flocs.

Funding This study was funded by the Youth Innovative Talent Project from the College and University in Guangdong Province (Grant no. 2018GkQNCX081), Natural Science Foundation of Guangdong province (No. 2018A030313363) and Shenzhen Science & Technology Project (JCYJ20180307155011964).

Availability of data and materials All data generated or analysed during this study are included in this published article (and its supplementary information files).

Declarations

Ethics approval and consent to participate Not applicable.

Consent for publication Not applicable.

Competing interests The authors declare no competing interests.

References

Ahmad SZN, Gheethi AA, Hamdan R, Othman N (2020) Efficiencies and mechanisms of steel slag with ferric oxides for removing phosphate from wastewater using a column filter system. Environ Sci Pollut Res 27:35184–35194

Antelo J, Avena M, Fiol S, López R, Arce F (2005) Effects of pH and ionic strength on the adsorption of phosphate and arsenate at the goethite–water interface. J Colloid Interface Sci 285:476–486

Bouzek K, Schmidt MJ, Wragg AA (1999) Influence of anode material composition on the stability of electrochemically-prepared ferrate(VI) solutions. J Chem Technol Biotechnol 74:1188–1194

Cameron AJ, Liss PS (1984) The stabilization of "dissolved" iron in freshwaters. Water Res 18:179–185

Charfi A, Sahnoun RD, Bouaziz J (2013) Characterization and mechanical properties of phosphate-kaolin clay. Powder Technol 235:633–639

Chen G, Lam WWY, Lo PK, Man WL, Chen LJ, Lau KC, Lau TC (2018) Mechanism of water oxidation by ferrate(VI) at pH 7-9. Chem Eur J 24:18735–18742

Chitrakar R, Tezuka S, Sonoda A, Sakane K, Ooi K, Hirotsu T (2006) Phosphate adsorption on synthetic goethite and akaganeite. J Colloid Interface Sci 298:602–608

Cho HM, Kim JH, Kim G (2019) Desorption of phosphate on sandy sediments by silicate in groundwater. Geochim Cosmochim Acta 257:184–190

Chu YB, Li M, Liu JW, Xu W, Cheng SH, Zhao HZ (2019) Molecular insights into the mechanism and the efficiency-structure relationship of phosphorus removal by coagulation. Water Res 147:195–203

Deng YX, Weng LP, Li YT, Ma J, Chen YL (2019) Understanding major NOM properties controlling its interactions with phosphorus and arsenic at goethite-water interface. Water Res 157:372–380

Doelsch E, Stone WEE, Petit S, Masion A, Rose J, Bottero JY, Nahon D (2001) Speciation and crystal chemistry of Fe (III) chloride hydrolyzed in the presence of SiO_4 ligands. 2. Characterization of Si-Fe aggregates by FTIR and 29Si solid-state NMR. Langmuir 17:1399–1405

Dong SY, Mu Y, Sun XH (2019) Removal of toxic metals using ferrate (VI): a review. Water Sci Technol 80:1213–1225

Hu YW, Shen L, Ren XQ, Bi YH, Hu BW, Wang BL (2020) Properties of CaO_2 for H_2O_2 release and phosphate removal and its feasibility in controlling Microcystis blooms. Environ Sci Pollut Res 27:35239–35248

Huang ZS, Wang L, Liu YL, Jiang J, Xue M, Xu CB, Zhen YF, Wang YC, Ma J (2018) Impact of phosphate on ferrate oxidation of organic compounds: An underestimated oxidant. Environ Sci Technol 52:13897–13907

Ilić B, Radonjanin V, Malešev M, Zdujić M, Mitrović A (2016) Effects of mechanical and thermal activation on pozzolanic activity of kaolin containing mica. Appl Clay Sci 123:173–181

Inan H, Alaydin E (2014) Phosphate and nitrogen removal by iron produced in electrocoagulation reactor. Desalin Water Treat 52:1396–1403

Kralchevska RP, Prucek R, Kolařík J, Tuček J, Machala L, Filip J, Sharma VK, Zbořil R (2016) Remarkable efficiency of phosphate removal: Ferrate (VI)-induced in situ sorption on core-shell nanoparticles. Water Res 103:83–91

Lartiges B, El-Samrani AG, Montargès-Pelletier E, Bihannicc I, Brioisd V, Michote L (2019) Aggregating ability of ferric chloride in the presence of phosphate ligand. Water Res 194:114960

Li WT, Zhou JZ, Zhang J, Zhang J, Xu YF, Qian GR (2013) pH-Dependent improvement of pyrophosphate removal on amorphous ferric hydroxide by incorporating Ca^{2+}. Chem Eng J 225:372–377

Lin ZG, Chen J (2021) Magnetic Fe_3O_4@MgAl-LDH@La(OH)(3) composites with a hierarchical core-shell structure for phosphate removal from wastewater and inhibition of labile sedimentary phosphorus release. Chemosphere 264:128511

Lin B, Hua M, Zhang YY, Zhang WM, Lv L, Pan BC (2017) Effects of organic acids of different molecular size on phosphate removal by HZO-201 nanocomposite. Chemosphere 166:422–430

Nakarmi A, Chandrasekhar K, Bourdo SE, Watanabe F, Guisbiers G, Viswanathan T (2020) Phosphate removal from wastewater using novel renewable resource-based, cerium/manganese oxide-based nanocomposites. Environ Sci Pollut Res 27:36688–36703

Prucek R, Tucek J, Kolarik J, Hušková I, Filip J, Varma RS, Sharma VK, Zbořil R (2015) Ferrate(VI)-prompted removal of metals in aqueous media: mechanistic delineation of enhanced efficiency via metal entrenchment in magnetic oxides. Environ Sci Technol 49:2319–2327

Saikial BJ, Parthasarathy G (2010) Fourier transform infrared spectroscopic characterization of kaolinite from assam and meghalaya, northeastern India. J Mod Phys 1:206–210

Vikrant K, Kim KH, Ok SY, Tsang DCW, Tsang YF, Giri BS, Singh RS (2018) Engineered/designer biochar for the removal of phosphate in water and wastewater. Sci Total Environ 616-617:1242–1260

Wang XM, Phillips BL, Boily JF, Hu YF, Hu Z, Yang P, Feng XH, Xu WQ, Zhu MQ (2019) Phosphate sorption speciation and precipitation mechanisms on amorphous aluminum hydroxide. Soil Syst 3:20

Wang XS, Liu YL, Xu SY, Zhang J, Li J, Song H, Zhang ZX, Wang W, Ma J (2020) Ferrate oxidation of phenolic compounds in iodine containing water: Control of iodinated aromatic products. Environ Sci Technol 54:1827–1836

Wilfert P, Kumar PS, Korving L, Witkamp GJ, van Loosdrecht MCM (2015) The relevance of phosphorus and iron chemistry to the recovery of phosphorus from wastewater: A review. Environ Sci Technol 49:9400–9414

Wu MY, Yu WZ, Qu JH, Gregory J (2019) The variation of flocs activity during floc breakage and aging, adsorbing phosphate, humic acid and clay particles. Water Res 155:131–141

Xu Y, Liu TJ, Huang YK, Zhu JY, Zhu RL (2020) Role of phosphate concentration in control for phosphate removal and recovery by layered double hydroxides. Environ Sci Pollut Res 27:16612–16623

Yang Q, Wang XL, Luo W, Sun J, Xu QX, Zhao JW, Wang S, Yao FB, Wang DB, Li XM, Zeng GM (2018) A Effectiveness and mechanisms of phosphate adsorption on iron-modified biochars derived from waste activated sludge. Bioresour Technol 247:537–544

Yang T, Wang L, Liu YL, Zhang W, Cheng HJ, Liu MC, Ma J (2020) Ferrate oxidation of bisphenol F and removal of oxidation products with ferrate resulted particles. Chem Eng J 383:123167

Yasipourtehrani S, Strezov V, Evans T (2019) Investigation of phosphate removal capability of blast furnace slag in wastewater treatment. Sci Rep 9:7498–7506

Yu FM, Li CM, Dai CL, Liu KH, Li Y (2020) Phosphate: Coupling the functions of fertilization and passivation in phytoremediation of manganese-contaminated soil by polygonum pubescens blume. Chemosphere 260:127651

Zhang YY, Pan BC, Shan C, Gao X (2016) Enhanced phosphate removal by nanosized hydrated La(III) oxide confined in cross-linked Polystyrene Networks. Environ Sci Technol 50:1447–1454

Zhang X, Gang DD, Sun PZ, Lian Q, Yao H (2020a) Goethite dispersed corn straw-derived biochar for phosphate recovery from synthetic urine and its potential as a slow-release fertilizer. Chemosphere 262:127861

Zhang ZR, Yu HQ, Zhu RX, Zhang X, Yan LG (2020b) Phosphate adsorption performance and mechanisms by nanoporous biochar-iron oxides from aqueous solutions. Environ Sci Pollut Res 27:28132–28145

Zhao JW, Xin MX, Zhang J, Sun YJ, Luo SY, Wang HW, Wang YA, Bi XJ (2020) Diclofenac inhibited the biological phosphorus removal: Performance and mechanism. Chemopshere 243:125380

Publisher's note Springer Nature remains neutral with regard to jurisdictional claims in published maps and institutional affiliations.